Biosensors and Bioelectronics 80 (2016) 647–653

Contents lists available at ScienceDirect

Biosensors and Bioelectronics

journal homepage: www.elsevier.com/locate/bios

Using DNA devices to track anticancer drug activity

Dimithree Kahanda [a], Gaurab Chakrabarti [b], Marc A. Mcwilliams [a], David A. Boothman [b], Jason D. Slinker [a,*]

[a] Department of Physics, The University of Texas at Dallas, 800 W. Campbell Rd., PHY 36, Richardson, TX 75080, United States
[b] Departments of Pharmacology, Oncology and Radiation Oncology, Laboratory of Molecular Stress Responses and the Simmons Comprehensive Cancer Center, University of Texas Southwestern Medical Center, ND2.210K 601 Forest Park Drive, Dallas, TX 75390-8807, United States

ARTICLE INFO

Article history:
Received 18 November 2015
Received in revised form
5 February 2016
Accepted 9 February 2016
Available online 12 February 2016

Keywords:
Electrochemical sensor
DNA repair
Biosensor
Base-excision repair
Oxidative damage

ABSTRACT

It is beneficial to develop systems that reproduce complex reactions of biological systems while maintaining control over specific factors involved in such processes. We demonstrated a DNA device for following the repair of DNA damage produced by a redox-cycling anticancer drug, beta-lapachone (β-lap). These chips supported ß-lap-induced biological redox cycle and tracked subsequent DNA damage repair activity with redox-modified DNA monolayers on gold. We observed drug-specific changes in square wave voltammetry from these chips at therapeutic ß-lap concentrations of high statistical significance over drug-free control. We also demonstrated a high correlation of this change with the specific ß-lap-induced redox cycle using rational controls. The concentration dependence of ß-lap revealed significant signal changes at levels of high clinical significance as well as sensitivity to sub-lethal levels of ß-lap. Catalase, an enzyme decomposing peroxide, was found to suppress DNA damage at a NQO1/catalase ratio found in healthy cells, but was clearly overcome at a higher NQO1/catalase ratio consistent with cancer cells. We found that it was necessary to reproduce key features of the cellular environment to observe this activity. Thus, this chip-based platform enabled tracking of ß-lap-induced DNA damage repair when biological criteria were met, providing a unique synthetic platform for uncovering activity normally confined to inside cells.

1. Introduction

There is a desperate need to develop highly selective and efficacious agents for patients with traditionally drug-resistant cancers. Conventional DNA-damaging drugs, such as cisplatin, methotrexate, and doxorubicin, are widely used, but do not offer tumor-selectivity and suffer from a number of resistance pathways (Cheung-Ong et al., 2013; Karran, 2001). Cancer treatments that use inherent differences in cancer versus normal cells to induce selective DNA damage represent a promising strategy for avoiding common therapeutic resistances. Strategies are now emerging that involve drugs that respond to overexpression of enzymes and inherent differences in reactive oxygen species (Cao et al., 2014; Vadukoot et al., 2014). Quantifying and maximizing the effectiveness of these cancer-selective DNA-damaging drugs necessitates understanding chemical alterations of DNA and DNA-protein interactions arising from the subsequent repair processes (Rauf et al., 2005).

Currently, we are exploring the mechanism of action of a drug that exploits cancer-specific overexpression of NAD(P)H:quinone oxidoreductase 1 (NQO1) for tumor-selective 'bioactivation' due to its great potential for efficacy against a number of aggressive solid tumors (Huang et al., 2016). NQO1 metabolizes unique quinones, such as ß-lapachone (ß-lap), to selectively kill cancer cells. NQO1 attempts to detoxify this drug in a two-electron oxidoreduction, changing it to the unstable hydroquinone (HQ) form. However, this ß-lap form is rapidly and non-enzymatically converted to parental drugs, allowing for multiple rounds of cytoplasmic redox cycling as illustrated in Fig. 1A. For each mole of ß-lap, ~60 mol of $NAD(P)^+$ are used to ultimately create hydrogen peroxide (H_2O_2) in two minutes (Bey et al., 2013). H_2O_2, a long-lived reactive oxygen species (ROS), subsequently causes oxidative DNA base damage, such as 8-oxoguanine defects, which is augmented by the presence of iron. This damage triggers specific, but overlapping, DNA repair processes, generating DNA base damage (and subsequent abasic sites), as well as single- and double-DNA strand breaks that hyperactivate poly(ADP-ribose) polymerase 1 (PARP1), ultimately leading to selective cancer programmed necrosis. NQO1 is constitutively over-expressed in most solid cancers, particularly in

Abbreviations: β-lap, β-lapachone; NQO1, NADH dependent quinone oxidoreductase 1; NADH, nicotinamide adenine dinucleotide; H_2O_2, hydrogen peroxide; SWV, square wave voltammetry; WM, well-matched DNA sequence; HPLC, high performance liquid chromatography; T_M, melting temperature

* Corresponding author.
E-mail address: slinker@utdallas.edu (J.D. Slinker).

http://dx.doi.org/10.1016/j.bios.2016.02.026
0956-5663/

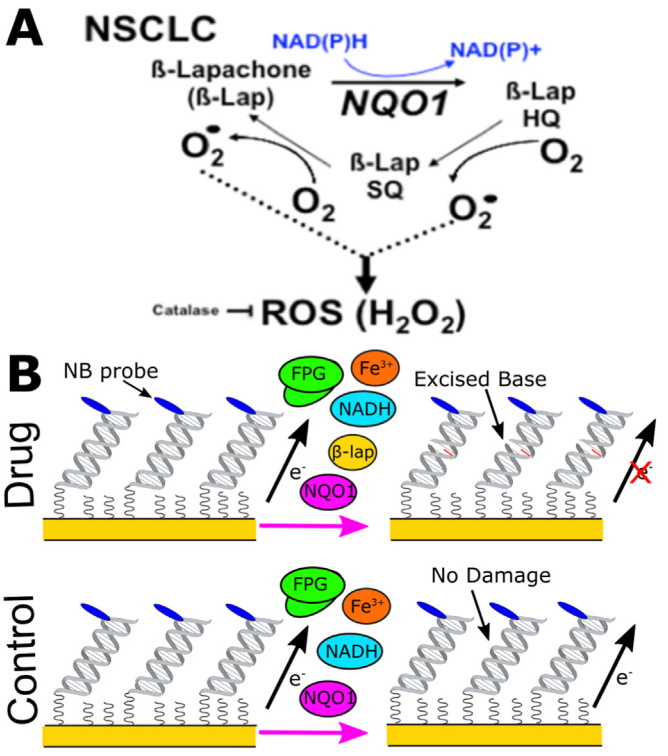

Fig. 1. (A) The futile redox cycle associated with β-lap in the presence of high levels of NQO1 and NADH. NQO1 converts β-lap to its hydroquinone form (HQ), which is unstable and spontaneously reverts through its semiquinone (SQ) form back to its parental drug in a spontaneous two step reaction using 2 O_2 that generates superoxide. Superoxide is then converted to H_2O_2 by superoxide dismutase (SOD). Since most solid tumors have high NQO1 levels with low levels of catalase, high pools of H_2O_2 can migrate to the cell nucleus and damage DNA when iron is present by the standard Fenton reaction. (B) Illustration of tracking β-lapachone (ß-lap) drug activity with DNA chips against a control with no β-lapachone. Experimental electrodes are treated with all of the components to generate ß-lap-induced DNA damage and subsequent repair activity, leading to lower signals.

non-small cell lung (> 85% show 10- to 50-fold elevations relative to normal tissue), pancreatic (~85% have 10- to 100-fold elevations), prostate (~60% have 5- to 100-fold elevations), and breast (~60% have 5- to 100-fold elevations) cancers (Bey et al., 2007; Cao et al., 2014; Chakrabarti et al., 2015a; Dong et al., 2010; Huang et al., 2012, 2013; Moore et al., 2015). Importantly, many of these same tumors concomitantly express low catalase levels compared to normal tissue (Chakrabarti et al., 2015b), so H_2O_2 levels generated by the drug are relatively long-lived compared to most reactive oxygen species. Furthermore, ß-lap-induced cell death avoids many resistance pathways, as studies show that the cell death induced is: (i) not dependent on the particular p53 status of the cancer cell; (ii) independent of cell cycle status; (iii) not affected by losses in expression of Bak and/or Bax; (iv) not affected by oncogenic driver or carrier mutations; and (v) not influenced by loss of caspases (Cao et al., 2014; Chakrabarti et al., 2015a; Huang et al., 2012, 2013; Moore et al., 2015). β-Lap has produced apparent cures of cancers in mice, and a modified form (ARQ761) is currently under several Phase I/Ib clinical trials. Thus, detecting its activity and gaining understanding of its functionality have potential health implications for the diagnosis and treatment of most solid cancers due to their NQO1 overexpression.

A challenge of detecting β-lap-induced DNA damage and its repair is the difficulty to selectively distinguish the protein activity of the removal of base defects from DNA, particularly 8-oxoguanine and similar oxidative damage. Sensing the repair activity of this damage is complicated by the fact that repair enzymes that fix 8-oxoguanine base lesions bind to DNA nonspecifically, such that enzymatic binding and excision activity are decoupled. 8-Oxoguanine itself has been distinguished by GC–MS and HPLC-coupled electrochemical detection (Abalea et al., 1999; Ivandini et al., 2007; Ravanat et al., 1998; Rebelo et al., 2004), and electrochemical devices were used to indirectly study DNA damage (Cahova-Kucharikova et al., 2005; Harfield et al., 2011; Havran et al., 2008; Oliveira-Brett et al., 2002; Wang et al., 1997). However, these techniques and devices have not offered a real-time quantitative measure of repair of oxidative DNA damage. Other electrical and electrochemical devices were used to follow DNA-binding drug interactions (Ibrahim, 2001; Wang et al., 1998), but unlike these studies, β-lap indirectly damages DNA.

To follow the DNA damaging activity of β-lap and subsequent DNA repair activity, we utilized electrochemical devices to simulate features of the cellular environment in a controlled format (Figs. 1B and 2). In particular, we used DNA-based electrochemical devices to naturally recognize DNA damage and repair activity, and transduce this event through changes in charge transport reactions. DNA was bound to electrodes on chips, and a redox probe at the top of the DNA reported charge transfer through the DNA (Gorodetsky et al., 2008a). Changes in the DNA structure, such as removal of a damaged base by a repair enzyme, lowered the voltammetry peak. We recently reported such an assay that detects base excision repair (BER) of oxidized bases sensitively (down to nanograms of the enzyme), selectively (against undamaged controls), and in real-time with the natural substrate (McWilliams et al., 2014). Here, we demonstrate the observation of drug-specific damage associated with therapeutic levels of the anticancer agent, ß-lapachone (ß-lap). This assay possessed key features to reproduce the biological redox cycle associated with the drug and BER of drug-induced damage. We pursued a thorough understanding of the electrochemical signals associated with cofactors and reaction pathways on the chip. We closely matched the underlying biology with the chip to observe drug-selective activity.

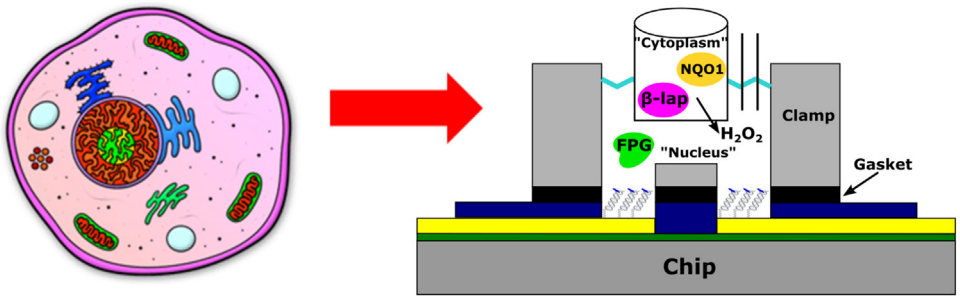

Fig. 2. Illustration of the concept of using DNA modified chips to mimic features of a cellular environment.

2. Materials and methods

2.1. Synthesis of oligonucleotides

Thiolated sequences were obtained from Integrated DNA Technologies (IDT). The thiol linker used was derived from the Glen Research thiol-modifier C6 S–S phosphoramidite. The DNA containing the Nile blue (NB) precursor base, a 5-[3-acrylate NHS ester] deoxyuridine phosphoramidite from Glen Research, was purchased from Trilink BioTechnologies and the dye covalently coupled under ultramild conditions according to established procedures (Gorodetsky et al., 2008b). The double stranded DNA monolayers utilized were from the 17mer sequence 3′-CTCTATATTTCGTGCGT$_{NB}$-5′ and the fully complementary sequence 5′-(C6 thiol)-GAGATATAAAGCACGCA-3′, where T_{NB} notes the position of a Nile blue modified thymine.

2.2. Purification and characterization of oligonucleotides

All oligonucleotides were purified *via* two rounds of high performance liquid chromatography (HPLC) on a Shimadzu LC-20 AD instrument outfitted with an SIL-20A autosampler and an SPD-M20A diode array detector. In the first purification round, DNA oligonucleotides with the 4,4′-dimethoxytrityl group on were eluted, while in the second purification round, DNA oligonucleotides with the 4,4′-dimethoxytrityl group off (removed according to Glen Research procedures for each strand) were purified, each according to previous reports (McWilliams et al., 2015; Wohlgamuth et al., 2014). The identity of the desired products was confirmed by matrix assisted laser desorption ionization time-of-flight mass spectrometry (MALDI-TOF) on a Shimadzu Axima Confidence mass spectrometer.

2.3. Preparation of duplex DNA

The oligonucleotides were quantified *via* UV–visible spectroscopy on a Beckman DU-800 UV–visible spectrophotometer. Duplex DNA was prepared by mixing equimolar amounts of complementary strands and annealing the solution to 95 °C, followed by slow cooling to room temperature over a period of 90 min. The formation of duplex DNA was verified by temperature dependent absorbance measurements and melting temperature analysis.

2.4. Fabrication of devices

The chips/substrates featuring multiplexed gold electrodes for DNA self-assembly and electrochemical experiments were prepared as previously described (McWilliams et al., 2015; Slinker et al., 2010). In brief, 1 mm thick Si wafers featuring a 10,000 Å thick oxide layer (Silicon Quest, Inc.) were patterned *via* a two-layer process. For the first layer, the gold electrodes were deposited by a lift-off technique. Initially, the wafers were cleaned thoroughly in 1165 Remover (Microchem, Inc.) to remove organic impurities. SPR 220 3.0 photoresist (Microchem, Inc.) was then spin-cast at 2000 rpm onto the wafers and baked. The photoresist was in turn patterned with a Karl Suss MA6 contact aligner and a chrome photomask. Following post-exposure baking, the wafers were developed in AZ 300 MIF developer for 1 min and rinsed thoroughly with deionized water. A 100 Å Ti adhesion layer and a 1000 Å Au layer were deposited onto the wafers *via* electron beam physical vapor deposition. The wafers were then immersed in Remover PG (Microchem, Inc.) overnight and sonicated to complete metal lift-off. Subsequently, the wafers were baked again and cleaned by UV ozone treatment. For the second layer, SU-8 2002 photoresist was spin-cast onto the wafers at 3000 rpm, baked, and photopatterned as an insulator, thereby isolating the exposed gold working electrode areas from the contact pads. The wafers were then developed in SU-8 Developer (Microchem, Inc.) for 1 min and baked to permanently set the photoresist. Finally, the completed wafers were diced into 1-in. by 1-in. chips by hand with a diamond scribe and stored under vacuum. The resulting multiplexed electrodes allowed for the self-assembly of distinct DNA sequences in each quadrant of the chip, as facilitated by shallow wells of an associated rubber gasket and clamp assembly placed over the chip (See Supporting information Fig. 1). Each quadrant of four electrodes enabled each sequence to be tested with fourfold redundancy, facilitating direct, unambiguous comparisons between up to four different DNA monolayers (Slinker et al., 2010).

2.5. Self-assembly of DNA monolayers

The DNA monolayers were self-assembled onto gold electrode pads from a buffer solution [5 mM phosphate, 50 mM sodium chloride, pH=7] over a period of 12–18 h. Substrates were backfilled with mercaptohexanol for 1 h to remove nonspecifically bound DNA and then thoroughly rinsed with buffer to remove residual mercaptohexanol.

2.6. Electrochemistry of DNA monolayers

The multiplexed substrates were placed in the custom mount shown in Supporting information (Fig. 1), which was connected to electrochemical testing hardware (a CH Instruments CHI750D Electrochemical Analyzer and a CHI 684 Multiplexer). The electrochemical measurements were performed in pH 7.9 buffer containing 50 mM NaCl, 10 mM Tris–HCl, 10 mM $MgCl_2$, and 4 mM spermidine. The membranes used in the chip to separate “nuclear” from “cytoplasmic” cofactors were the microdialysis strips associated with the Pierce 96-well microdialysis plate, 3.5K molecular weight cutoff (MWCO) from Thermo Scientific. The formamidopyrimidine DNA glycosylase was purchased from New England Biolabs and exchanged to the device buffer using a Pierce mini-dialysis kit (3.5k MWCO, Thermo Scientific). ß-Lap (3,4-dihydro-2,2-dimethyl-2*H*-naphtho[1,2-*b*]pyran-5,6-dione) was synthesized, confirmed by NMR, dissolved in DMSO at 50 μmol/L, and concentrations verified by spectrophotometry (Pink et al., 2000). Recombinant human NAD(P)H:quinone oxidoreductase 1 (NQO1) was purchased from Abcam (ab59663) and used as received. NADH was purchased from Sigma Aldrich (N8129) and used as received. Apo-transferrin was purchased from Alfa Aesar and used as received. Catalase was purchased from EMD Millipore and used as received.

3. Results and discussion

3.1. Electrochemical DNA device platform

Our approach to track β-lap-induced, NQO1-dependent DNA damage and its subsequent repair activity is illustrated in Figs. 1B and 2, and Supporting information Fig. 1. We prepared 16-electrode devices with fully well-matched, undamaged DNA monolayers bearing redox probes on gold electrodes. These devices utilize a clamp and gasket assembly that supports two wells over the chip, dividing them into halves of 8 electrodes each with isolated solution wells for different biological treatments. One-half of this chip is the drug side, with all cofactors necessary for generation of ß-lap-induced H_2O_2, DNA damage, and damage repair. The control side is where all cofactors except the drug are present. Dialysis membranes (Supporting information Fig. 1B) are supported over each half of the chip to separate cytoplasmic from nuclear components to represent the underlying biology of the

system. Under this arrangement, β-lapachone, in the presence of biologically-high levels of NQO1 and NADH produces superoxide that converts to H_2O_2, which, in the presence of iron in the vicinity of DNA causes oxidative DNA damage, such as 8-oxoguanine (Chakrabarti et al., 2015b). This damage is repaired on our chip by formamidopyrimidine glycosylase (FPG), an 8-oxoguanine repair enzyme, lowering the voltammetry signal.

3.2. Verification of sensor operational principles

To verify the operation of this sensor, before performing the full experiments noted in Fig. 2, we investigated the individual cofactors and partial reaction pathways to ensure that we were monitoring NQO1-dependent DNA damage and subsequent BER activity mediated by FPG, and anticipate device signal changes. Notably, we showed that these sensors selectively followed repair of 8-oxoguanine-modified DNA by FPG in our previous work (McWilliams et al., 2014). This is important as glycosylases, such as FPG, bind to DNA nonspecifically but excise bases with high damage specificity, requiring sensors that transduce base excision, rather than DNA binding, to distinguish activity over controls. Subsequently, we verified that this assay responded to ß-lap-induced DNA lesions, and functioned specifically in the presence of peroxide and iron. To address this, we induced DNA damage by the Fenton reaction (Fig. 3). At 1 mM H_2O_2, the damage produced a change in square wave voltammetry (SWV) peak height that was approximately a factor of two above the nonspecific binding of 200 units/mL (400 nM) FPG. Importantly, this shows both compatibility with ROS species produced by the drug, as well as responsivity to environmental oxidative damage. The redox chemistry of NADH was measured, and oxidation to NAD^+ was observed at positive potentials versus Ag/AgCl, far from the Nile Blue redox probe (Supporting information Fig. 2). β-Lap is reduced around −0.360 V versus Ag/AgCl (Supporting information Fig. 3), which is close to the Nile Blue probe, but does not seem to interfere with the probe signal, and can ultimately be washed away post-reaction.

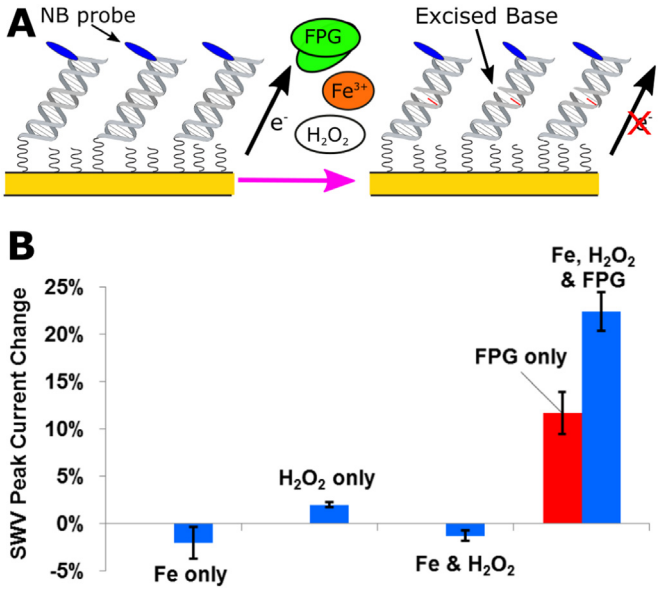

Fig. 3. (A) Illustration of the Fenton reaction experiment. Iron (III) chloride and peroxide are added to the chip, generating oxidative damage. Addition of FPG, an 8-oxoguanine repair enzyme, removes damaged bases, lowering the redox signal from charge transport. (B) SWV peak current signal loss of initially undamaged, chip-bound DNA monolayer to successive addition of 2 mM $FeCl_3$, 1 mM H_2O_2, and 200 units/mL FPG, relative to a control subjected to 200 units/mL FPG only. This was performed in pH 7.9 buffer containing 50 mM NaCl, 10 mM Tris–HCl, 10 mM $MgCl_2$, and 4 mM spermidine.

3.3. Investigation of drug activity with controls

We performed electrochemical experiments of DNA chips as illustrated in Fig. 1B. Drug-specific changes in square wave voltammetry (SWV) observed from a DNA chip is shown in Fig. 4. First, we measured the SWV signals of each half of the chip before addition of any components and averaged over the electrodes of each. Both halves exhibited the Nile Blue redox peak at −0.250 V vs. Ag/AgCl (Gorodetsky et al., 2008b; McWilliams et al., 2015) and peak heights of ~35 nA each (thin traces of each graph). Devices were then treated on both sides of the chip with NQO1 (50 nM, biologically relevant level, in dialysis strip), NADH (200 μM), and iron (2 mM). Subsequently, β-lap (2.5 μM, biologically lethal dose) was added to one-half of the chip, labeled the “drug” side, while the other side was kept drug-free as a control (“no drug”). On the drug side, all factors were present to activate NQO1-dependent futile redox cycle of ß-lap (Fig. 1A), generating approximately 300 μM levels of peroxide and subsequent oxidative damage such as 8-oxoguanine. In contrast, the drug free side presumably remained free of damage as the drug futile redox cycle was not activated in the absence of ß-lap. After rinsing both sides of the chip with buffer, they were then treated with 300 units/mL FPG (600 nM, added outside the dialysis strip), which nonspecifically binds to both monolayers, but excises oxidative damage from the drug side, leading to additional signal loss. The resulting SWV signals are shown in Fig. 4 (Thick traces). The redox peaks of ß-lap-exposed monolayers were significantly diminished due to FPG activity, while the drug-free electrodes retain most of their signal. We performed five experimental trials of β-lap treatment on different chips, with each trial averaged across four electrodes, and the resulting SWV peak height changes are summarized in Fig. 5 along with the associated controls. The drug-treated monolayers showed an average signal loss of 57 ± 3%, while the drug-free sides changed only 36 ± 3% (*t*-test *p*-value of 0.00017). Thus, the drug-treated side showed signal changes significantly higher than the untreated side. Given the anticipated generation of H_2O_2 of ~0.3 mM, this change is consistent with responses from the stand-alone Fenton reaction of higher H_2O_2 concentration (Fig. 3). The change observed in drug-free electrodes is associated with nonspecific binding by FPG (McWilliams et al., 2014). Additional controls were performed with β-lap present, but with other factors of the futile redox cycle removed. Removal of NQO1 or NADH from the drug-active mixture returned the SWV signals to drug-free levels (Fig. 5). Thus, the significant changes upon drug inclusion are consistent with the oxidative damage generated by redox cycling with NQO1 as facilitated by NADH.

3.4. Sensor concentration dependence

The β-lap concentration dependence of the signal change was investigated across three specific concentrations: a dose typically lethal to cancer cells (2.5 μM, such as MCF-7 breast cancer cells (Wuerzberger et al., 1998; Cao et al., 2014)), a dose at the threshold of activity (1.0 μM), and at an order of magnitude below this *in vivo* activity threshold (0.10 μM). Each concentration was measured against a drug-free control on the chip and normalized against the nonspecific change, $(C-D)/C$, where C is the change associated with the drug free control and D is the change associated with the drug-treated electrodes. As seen in Fig. 6, an increasing trend of signal change is associated with the increase in concentration. Two features are notable about these data. Interestingly, there is a large difference associated with the change from the threshold to the lethal concentration, which is an encouraging result for using this technology to correlate with *in vivo* activity. These data strongly suggest that BER can create DNA damage that would then be detected by PARP1, and result in hyperactivation downstream,

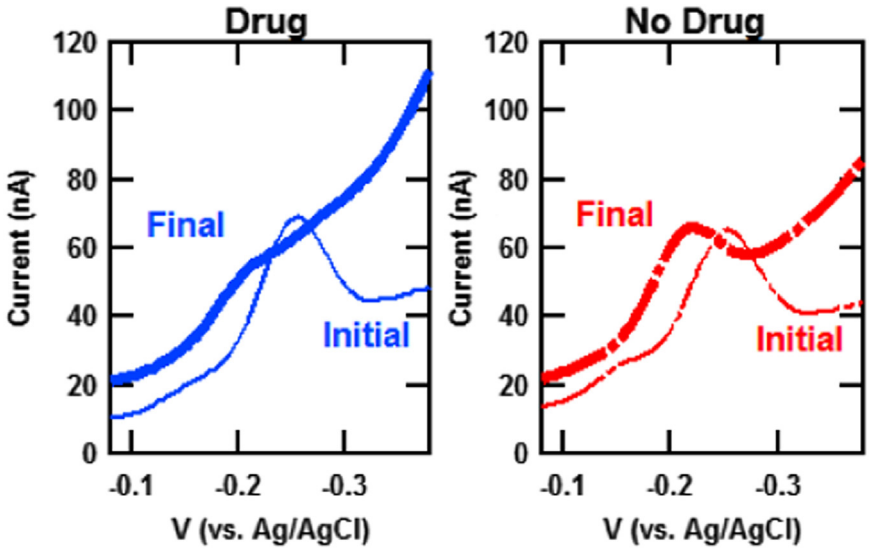

Fig. 4. Square wave voltammetry (SWV) of DNA chips before (thin trace) and after (thick trace) addition of NQO1, NADH, iron, and FPG, with (blue, solid) or without (red, dashed) the β-lap drug, averaged over 4 electrodes each on a chip. DNA damage from the drug-treated electrodes causes significant loss of the voltammetry peak, while significantly less change is seen on the untreated side. (For interpretation of the references to color in this figure legend, the reader is referred to the web version of this article.)

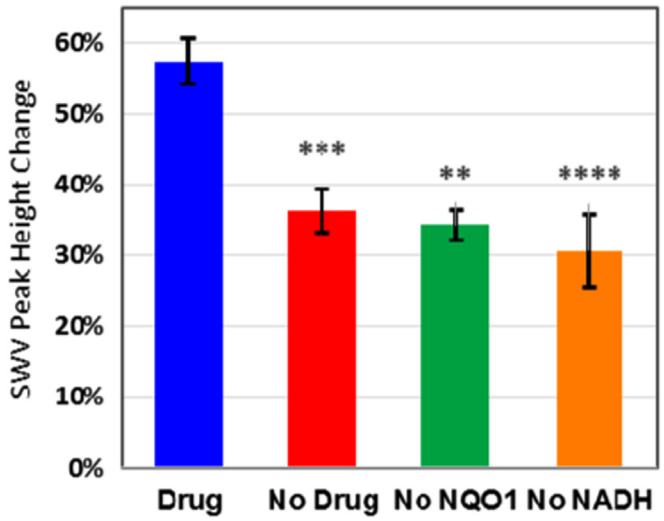

Fig. 5. Change in square wave voltammetry peak height for device treatment with (Drug) and without (No Drug) the β-lap drug (2.5 μM) with all other cofactors, as well as controls with without NQO1 or NADH. Error bars represent standard error across electrodes. Asterisks represent *p*-values from student's *t*-tests for controls against the Drug data as follows: $^{*}p \leq 0.05$; $^{**}p \leq 0.01$; $^{***}p \leq 0.001$; $^{****}p \leq 0.0001$.

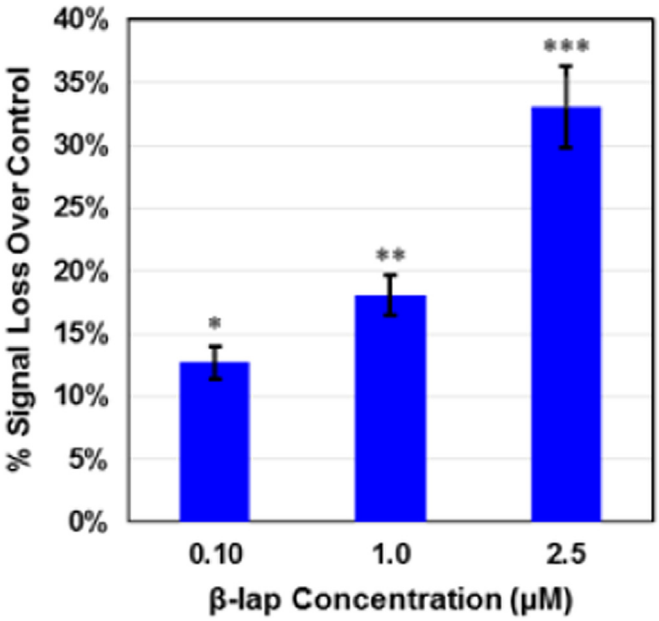

Fig. 6. Change in square wave voltammetry peak height as percent signal loss relative to a no drug control for devices treated with three concentrations of β-lap drug along with NQO1 (50 nM), NADH (200 μM), iron (2 mM), and FPG (300 nM). Error bars represent the standard error across electrodes. Asterisks represent *p*-values from student's *t*-tests against co-tested drug-free controls as follows: $^{*}p \leq 0.05$; $^{**}p \leq 0.01$; $^{***}p \leq 0.001$; $^{****}p \leq 0.0001$.

consistent with the mode of cell death caused by ß-lap (Chakrabarti et al., 2015b). Secondly, we can clearly see changes above the nonspecific threshold well below the *in vivo* activity threshold at 0.10 μM β-lap. The chip assay conducted in this format does not have various detoxification pathways or cellular uptake barriers that serve to counteract β-lap activity *in vivo*, but importantly could be useful in following combinatorial approaches that exploit these subthreshold β-lap levels. We present a detoxification pathway in the next experiment.

3.5. Study of drug detoxification by catalase

Finally, in cells, H_2O_2 can be decomposed by enzymes such as catalase. Altered catalase expression was shown to lead to β-lap resistance (Bey et al., 2013), and comparative studies show that catalase plays a dominant role in H_2O_2 regulation (Jones et al., 1981). Recent work has shown catalase levels to be lowered in many solid tumors (Chakrabarti et al., 2015b), which, together with NQO1 overexpression, contributes to the selective activity of β-lap. To investigate this effect, we performed two experiments with catalase (Fig. 7), one with relatively low levels of catalase (10 activity units/ml, 0.0030 nmol/ml, 3.0 nM) and high levels of NQO1 (50 nM), consistent with cancerous cells, and another one with high levels of catalase (100 activity units/ml, 0.030 nmol/ml, 30 nM) and lower levels of NQO1 (5 nM), representative of a healthy cell. These ratios were selected from the relative expression levels of these enzymes from repeated trials of solid tumors (Bey et al., 2007; Cao et al., 2014; Chakrabarti et al., 2015a; Dong

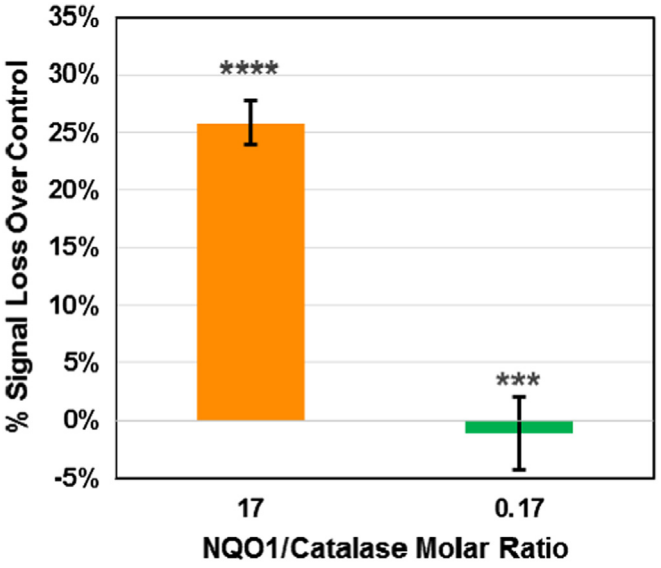

Fig. 7. Change in square wave voltammetry peak height as percent signal loss relative to a no drug control for devices treated with differing ratios of NQO1 to catalase, which decomposes H_2O_2, along with NADH (200 μM), iron (2 mM), β-lap (2.5 μM), and FPG (300 nM). Error bars represent the standard error across electrodes. Asterisks represent *p*-values from student's *t*-tests against a co-tested drug-free control (17) or 2.5 μM β-lap full activity data (0.17) as follows: $^{*}p \leq 0.05$; $^{**}p \leq 0.01$; $^{***}p \leq 0.001$; $^{****}p \leq 0.0001$.

et al., 2010; Huang et al., 2012, 2013; Moore et al., 2015). Each experiment was conducted along with a drug-free control. In the case of high NQO1/catalase (17 molar ratio), signal losses very similar to those observed with no catalase present are observed. This indicates that the catalytic activity of the high levels of NQO1 is sufficient overcome catalase activity when catalase is underexpressed. In the case of low NQO1/catalase ratio (0.17), no signal loss is observed relative to control, consistent with decomposition of H_2O_2 by catalase as would be expected in a healthy cell. Thus, this device technology also enables study of drug abrogation pathways and experiments of high biological complexity.

3.6. Critical features for successful operation

Critical to the success of this assay was maintaining essential elements of the underlying biology. One such feature is that NQO1 is external to the nucleus in the cytoplasm, but delivers long-lived H_2O_2 levels that are readily membrane-soluble (Cao et al., 2014; Bey et al., 2013). We found it necessary to represent this nuclear segregation feature, as NQO1 inhibited FPG activity by some unknown mechanism (likely nonspecific protein–protein binding) if directly exposed to the DNA of the chip. NQO1 has been reported to bind p53 and regulate its degradation, so NQO1 may play a larger role in BER enzyme function (Anwar et al., 2003; Asher et al., 2002a,b). We, therefore, reproduced this nuclear segregation by adding dialysis strips as illustrated in Fig. 2 and Supporting information Figs. 1B and 1C. The conventional DNA-modified electrodes and repair proteins within the clamp may be considered the "nuclear" region of the chip, while components in the dialysis strip represent areas external to the nucleus in the cytoplasm. The dialysis membrane (3.5 kDa molecular weight cutoff) permits the interchange of peroxide (and other small molecules) across what would be the nuclear membrane of the conventional cell, but maintains segregation of the enzymes. Secondly, in some cases we found our Nile Blue redox signal to become unquantifiable due to iron-induced electrochemistry that could not be removed by simple rinsing of the chip surface (See Supporting information Fig. 4). Considering that iron uptake is enzymatically regulated in the cell (Crichton and Charloteaux-Wauters, 1987), we introduced iron to our chip coupled to transferrin. This enabled consistent recovery of the Nile Blue signal after drug treatment. Thus, we observed better performance as the environment of the cell was more closely matched by our device. Our data are consistent with a role of BER, specifically repair glycosylase activity, whose activity was required for ß-lap-induced lethality (Chakrabarti et al., 2015a, b). This demonstration of biological activity with these DNA devices in response to drug activity opens the possibility for additional biological study on this surface, such as discerning drug-induced cell death mechanisms. Furthermore, the low sample volumes (~100 to 200 μL) and clear readout offer potential for diagnosis of disease states and monitor of therapeutic progress.

4. Conclusion

We demonstrated a chip-based platform to follow the repair of DNA damage produced by a futile redox-cycling anticancer drug, beta-lapachone (β-lap). We observed ß-lap-specific changes in the square wave voltammetry signals of high statistical significance over drug-free controls and demonstrated high correlation of this change with the specific drug redox cycle through rational controls. The concentration dependence of ß-lap revealed significant signal changes at levels of high clinical significance as well as sensitivity to sub-lethal levels of ß-lap. Catalase was found to suppress DNA damage at a NQO1/catalase ratio found in healthy cells, but was clearly overcome at a higher NQO1/catalase ratio consistent with cancer cells. We found that reliable and reproducible signals were produced as conditions associated with the cellular environment were more closely matched by our device. Thus, this chip-based platform enables tracking of drug-induced damage repair processes when biological criteria are met, providing a unique synthetic platform for uncovering activity normally confined inside cells.

Acknowledgments

This work was performed in part at the UT Dallas Cleanroom Research Laboratory. This work was supported by startup funds from UT Dallas, a gift from Plexon, Inc., and NIH/NCI grant R01 102792 (DAB). The authors would like to thank Kuo-Yao Lin for his role in fabricating chips.

Appendix A. Supplementary material

Supplementary data associated with this article can be found in the online version at http://dx.doi.org/10.1016/j.bios.2016.02.026.

References

Abalea, V., Cillard, J., Dubos, M.P., Sergent, O., Cillard, P., Morel, I., 1999. Free Radic. Biol. Med. 26 (11 – 12), 1457–1466.
Anwar, A., Dehn, D., Siegel, D., Kepa, J.K., Tang, L.J., Pietenpol, J.A., Ross, D., 2003. J. Biol. Chem. 278 (12), 10368–10373.
Asher, G., Lotem, J., Kama, R., Sachs, L., Shaul, Y., 2002a. Proc. Natl. Acad. Sci. USA 99 (5), 3099–3104.
Asher, G., Lotem, J., Sachs, L., Kahana, C., Shaul, Y., 2002b. Proc. Natl. Acad. Sci. USA 99 (20), 13125–13130.
Bey, E.A., Reinicke, K.E., Srougi, M.C., Varnes, M., Anderson, V.E., Pink, J.J., Li, L.S., Patel, M., Cao, L., Moore, Z., Rommel, A., Boatman, M., Lewis, C., Euhus, D.M., Bornmann, W.G., Buchsbaum, D.J., Spitz, D.R., Gao, J., Boothman, D.A., 2013. Mol. Cancer Ther. 12 (10), 2110–2120.
Bey, E.A., Bentle, M.S., Reinicke, K.E., Dong, Y., Yang, C.-R., Girard, L., Minna, J.D., Bornmann, W.G., Gao, J., Boothman, D.A., 2007. Proc. Natl. Acad. Sci. USA 104 (28), 11832–11837.

Cahova-Kucharikova, K., Fojta, M., Mozga, T., Palecek, E., 2005. Anal. Chem. 77 (9), 2920–2927.
Cao, L., Li, L.S., Spruell, C., Xiao, L., Chakrabarti, G., Bey, E.A., Reinicke, K.E., Srougi, M. C., Moore, Z., Dong, Y., Vo, P., Kabbani, W., Yang, C.R., Wang, X., Fattah, F., Morales, J.C., Motea, E.A., Bornmann, W.G., Yordy, J.S., Boothman, D.A., 2014. Antioxid. Redox Signal. 21 (2), 237–250.
Chakrabarti, G., Gerber, D.E., Boothman, D.A., 2015a. Clin. Pharmacol. 7, 57–68.
Chakrabarti, G., Silvers, M.A., Ilcheva, M., Liu, Y., Moore, Z.R., Luo, X., Gao, J., Anderson, G., Liu, L., Sarode, V., Gerber, D.E., Burma, S., DeBerardinis, R.J., Gerson, S.L., Boothman, D.A., 2015b. Sci. Rep. 5, 17066.
Cheung-Ong, K., Giaever, G., Nislow, C., 2013. Chem. Biol. 20 (5), 648–659.
Crichton, R.R., Charloteaux-Wauters, M., 1987. Eur. J. Biochem. 164 (3), 485–506.
Dong, Y., Bey, E.A., Li, L.-S., Kabbani, W., Yan, J., Xie, X.-J., Hsieh, J.-T., Gao, J., Boothman, D.A., 2010. Cancer Res. 70 (20), 8088–8096.
Gorodetsky, A.A., Buzzeo, M.C., Barton, J.K., 2008a. Bioconjug. Chem. 19 (12), 2285–2296.
Gorodetsky, A.A., Ebrahim, A., Barton, J.K., 2008b. J. Am. Chem. Soc. 130 (10), 2924–2925.
Harfield, J.C., Toghill, K.E., Batchelor-McAuley, C., Downing, C., Compton, R.G., 2011. Electroanalysis 23 (4), 931–938.
Havran, L., Vacek, J., Cahova, K., Fojta, M., 2008. Anal. Bioanal. Chem. 391 (5), 1751–1758.
Huang, X., Dong, Y., Bey, E.A., Kilgore, J.A., Bair, J.S., Li, L.S., Patel, M., Parkinson, E.I., Wang, Y., Williams, N.S., Gao, J., Hergenrother, P.J., Boothman, D.A., 2012. Cancer Res. 72 (12), 3038–3047.
Huang, X., Dong, Y., Bey, E.A., Kilgore, J.A., Bair, J.S., Li, L.S., Patel, M., Parkinson, E.I., Wang, Y., Williams, N.S., Gao, J., Hergenrother, P.J., Boothman, D.A., 2013. Cancer Res. 72 (12), 3038–3047.
Huang, X., Ma, X., Huang, G., Moore, Z., Boothman, D., Kilgore, J.A., Williams, N.S., Gao, J., 2016. Cancer Cell (under review).
Ibrahim, M.S., 2001. Anal. Chim. Acta 443 (1), 63–72.
Ivandini, T.A., Honda, K., Rao, T.N., Fujishima, A., Einaga, Y., 2007. Talanta 71 (2), 648–655.
Jones, D.P., Eklöw, E., Thor, H., Orrenius, S., 1981. Arch. Biochem. Biophys. 210 (2), 505–516.
Karran, P., 2001. Carcinogenesis 22 (12), 1931–1937.
McWilliams, M.A., Anka, F.H., Balkus, K.J., Slinker, J.D., 2014. Biosens. Bioelectron. 54, 541–546.
McWilliams, M.A., Bhui, R., Taylor, D.W., Slinker, J.D., 2015. J. Am. Chem. Soc. 137 (34), 11150.
Moore, Z., Chakrabarti, G., Luo, X., Ali, A., Hu, Z., Fattah, F.J., Vemireddy, R., DeBerardinis, R.J., Brekken, R.A., Boothman, D.A., 2015. Cell Death Dis. 6, e1599.
Oliveira-Brett, A.M., Vivan, M., Fernandes, I.R., Piedade, J.A.P., 2002. Talanta 56 (5), 959–970.
Pink, J.J., Planchon, S.M., Tagliarino, C., Varnes, M.E., Siegel, D., Boothman, D.A., 2000. J. Biol. Chem. 275 (8), 5416–5424.
Rauf, S., Gooding, J.J., Akhtar, K., Ghauri, M.A., Rahman, M., Anwar, M.A., Khalid, A. M., 2005. J. Pharm. Biomed. 37 (2), 205–217.
Ravanat, J.L., Gremaud, E., Markovic, J., Turesky, R.J., 1998. Anal. Biochem. 260 (1), 30–37.
Rebelo, I.A., Piedade, J.A.P., Oliveira-Brett, A.M., 2004. Talanta 63 (2), 323–331.
Slinker, J.D., Muren, N.B., Gorodetsky, A.A., Barton, J.K., 2010. J. Am. Chem. Soc. 132 (8), 2769–2774.
Vadukoot, A.K., AbdulSalam, S.F., Wunderlich, M., Pullen, E.D., Landero-Figueroa, A. J., Mulloy, J.C., Merino, E.J., 2014. Bioorg. Med. Chem. 22 (24), 6885–6892.
Wang, J., Ozsoz, M., Cai, X.H., Rivas, G., Shiraishi, H., Grant, D.H., Chicharro, M., Fernandes, J., Palecek, E., 1998. Bioelectrochem. Bioenerg. 45 (1), 33–40.
Wang, J., Rivas, G., Ozsos, M., Grant, D.H., Cai, X.H., Parrado, C., 1997. Anal. Chem. 69 (7), 1457–1460.
Wuerzberger, S.M., Pink, J.J., Planchon, S.M., Byers, K.L., Bornmann, W.G., Boothman, D.A., 1998. Cancer Res. 58 (9), 1876–1885.
Wohlgamuth, C.H., McWilliarns, M.A., Mazaheripour, A., Burke, A.M., Lin, K.Y., Doan, L., Slinker, J.D., Gorodetsky, A.A., 2014. J. Phys. Chem. C 118 (50), 29084–29090.